Structure of collective states built on the $11/2^+$ isomer in ^{187}Os: Quasiparticle-plus-triaxial-rotor model and interpretation as tilted-precession bands

M. A. Sithole,[1,2,*] E. A. Lawrie,[2,1,†] L. Mdletshe,[3,2] S. N. T. Majola,[4,3,2] A. Kardan,[5] T. D. Bucher,[1,2] J. F. Sharpey-Schafer,[3] J. J. Lawrie,[2] S. S. Ntshangase,[3] A. A. Avaa,[2,6] R. A. Bark,[2] M. V. Chisapi,[2,7] P. Jones,[2] S. Jongile,[2,7] D. Kenfack,[2,7] T. C. Khumalo,[2,3] L. Makhathini,[2,7] K. L. Malatji,[2,7] B. Maqabuka,[1,2] S. H. Mthembu,[1,2] L. Msebi,[1,2] A. A. Netshiya,[1,2] G. O'Neill,[1,8] O. Shirinda,[2,9] P. M. Someketa,[10] and B. R. Zikhali[2,1,3]

[1]*Department of Physics, University of the Western Cape, P/B X17, Bellville 7535, South Africa*
[2]*iThemba LABS, National Research Foundation, PO Box 722, Somerset West 7129, South Africa*
[3]*Department of Physics, University of Zululand, P/B X1001, KwaDlangezwa 3886, South Africa*
[4]*Department of Physics, University of Johannesburg, PO Box 524, Auckland Park 2006, South Africa*
[5]*School of Physics, Damghan University, P.O.Box 36716-41167, Damghan, Iran*
[6]*School of Physics, University of the Witwatersrand, Johannesburg, 2000, South Africa*
[7]*Department of Physics, University of Stellenbosch, P/B X1, Matieland 7602, South Africa*
[8]*Department of Physics and Technology, University of Bergen, Allegaten 55, 5007 Bergen, Norway*
[9]*Department of Physical and Earth Sciences, Sol Plaatjie University, Private Bag X5008, Kimberly 8301, South Africa*
[10]*Department of Physics, University of Fort Hare, Private Bag X1314, King William's Town Rd, Alice 5700, South Africa*

(Received 11 May 2021; revised 10 June 2021; accepted 5 October 2021; published 21 October 2021)

Background: The shape of most nuclei is described by its quadrupole deformation (showing the deviation from spherical shape) and its triaxiality (showing the deviation from axial symmetry). Nuclei affected by triaxiality show additional collective rotational bands, called γ bands, that appear at low excitation energy. The γ bands can be caused by the precession of a nucleus with triaxial shape, but can also arise from small γ vibrations around an axially symmetric shape.
Purpose: The aim of this work is to search for new collective excitations in ^{187}Os in particular related with the γ degree of freedom.
Methods: The rotational structures of ^{187}Os were populated by the ^{186}W(^{4}He, 3n)^{187}Os reaction at a beam energy of 37 MeV. The measurements of γ - γ coincidences, angular distribution ratios and γ-ray intensities were performed using eleven Compton-suppressed Ge clover detectors.
Results: The previously known positive-parity band built on the $11/2^+$ isomer has been extended up and a new excited positive-parity band built above a $15/2^+$ state has been observed. The $11/2^+$ band was assigned a $\nu i_{13/2}$ configuration while the new $15/2^+$ band was associated with a coupling of the valence $i_{13/2}$ neutron with the γ band of the even-even core. The quasiparticle-plus-triaxial-rotor model calculations provide a good agreement with the experimental data for both bands. They describe the $15/2^+$ band as a collective excitation with respect to the $11/2^+$ band that corresponds to a precession of the intermediate nuclear axis similarly to the precession of a rotating top.
Conclusions: As shown by the calculations, the new rotational band can be understood as resulting from the three-dimensional rotation of a triaxially-deformed nucleus. However, a description based on the vibrations of a γ-soft nuclear shape should also be investigated in order to firmly establish the nature of the excited positive-parity band. Further studies able to distinguish between these alternative descriptions will be beneficial.

DOI: 10.1103/PhysRevC.104.044326

I. INTRODUCTION

Deformed axially-symmetric nuclei can generate angular momentum by collective rotation around an axis perpendicular to their symmetry axis. Such simple rotation in an even-even nucleus forms its ground-state rotational band. Nuclei with triaxial deformation (the three nuclear axes have different length) can rotate around all their three axes. Such simultaneous rotation in three dimensions (3D rotation) is more complex and in addition to the ground-state band generates some excited bands. To illustrate the nature of these bands, let us consider the rotational energy of a triaxial even-even nucleus,

$$E = \frac{\hbar^2}{2\Im_1}R_1^2 + \frac{\hbar^2}{2\Im_2}R_2^2 + \frac{\hbar^2}{2\Im_3}R_3^2, \quad (1)$$

where R_1, R_2, and R_3 are the rotational angular momenta along the three nuclear axes and $\Im_1$, $\Im_2$, and $\Im_3$ are the

*sitholemakuhaneabel@gmail.com
†elena@tlabs.ac.za

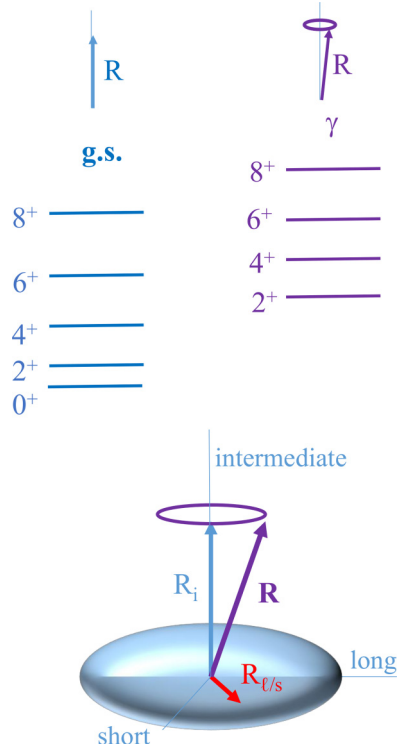

FIG. 1. Sketch illustrating the precession of the rotational angular momentum R around the intermediate axis of a triaxially-deformed nucleus. For the ground-state band the total rotational angular momentum R is approximately aligned along the intermediate axis, however it is tilted away from this axis and precesses around it for the γ bands, because these bands involve unfavoured rotation in the plane defined by the short and long nuclear axes.

corresponding moments of inertia. The rotation around the axis with largest moment of inertia is favoured, because it needs least energy for a given angular momentum. The dependence of the moments of inertia on the triaxial deformation γ, is usually described using the empirically supported [1] irrotational-flow model:

$$\Im_k = \Im_0 \sin^2\left(\gamma - k\frac{2\pi}{3}\right), \tag{2}$$

where k labels the three nuclear axes. The moment of inertia along the intermediate axis is largest.

The 3D rotation of triaxial even-even nuclei can be described schematically as follows. The ground-state band, which is the lowest-energy band, corresponds (approximately) to favoured rotations, where the rotational angular momentum increases along the intermediate axis. The 2^+ γ band, corresponds to dominant favoured rotation around the intermediate axis too, but also involves one unit of unfavoured rotation of $2\hbar$ in the plane defined by the short and long nuclear axes, as shown in Fig. 1. Therefore, while the rotational angular momentum is still increasing along the intermediate axis the total rotational angular momentum R is tilted away from it. The unfavoured rotation may have different projections on the short and long nuclear axes, the total rotational angular momentum R precesses around the intermediate axis, as illustrated in the bottom part of Fig. 1. Unfavoured rotation of $2\hbar$ and $4\hbar$ generates the 2^+ and 4^+ γ bands, respectively. The excitation energy of the γ bands strongly depends on the triaxial deformation γ; for nuclei with increasing triaxiality, the excitation energy of the γ bands decreases. While γ bands can be understood as generated by the precession of a deformed triaxial nucleus, they may also result from dynamical fluctuations, where the nuclear shape is axially symmetric on average, but vibrates with small amplitude with respect to the γ parameter. One-phonon γ vibration produces a 2^+ γ band, while 2-phonon γ vibration generates a 4^+ γ band. Gamma bands have been observed in many deformed nuclei and there is often a debate on whether these bands result from the rotation of a nucleus with rigid triaxial shape, or from the vibrations of a γ-soft nuclear shape. While some of the critical characteristics pertaining to the microscopic structure of γ bands remain elusive, it is worth noting that wherever they are observed in the transitional rare-earth region [2–9], one of their notable features is that their excitation energy, runs parallel to that of their intrinsic configuration (usually the ground-state band in even-even nuclei), as a function of spin.

The stable even-even osmium nuclei show excited rotational bands, including γ bands, at low excitation energy. This suggests that for these isotopes the γ degree of freedom is important. The observed 2^+ and 4^+ γ bands together with the excited bands built on the second 0^+ states in the Os isotopes with N = 106–116 are illustrated in Fig. 2. As the neutron number N increases both the quadrupole deformation and the excitation energies of the γ band decrease steadily and the 2_2^+ state in ^{192}Os has the lowest excitation energy observed in the entire nuclear chart. In contrast the excitation energies of the excited 0_2^+ band remain almost constant for these isotopes varying in the range of $E_{\rm exc} = 1096$ to 912 keV, see Fig. 2. In addition candidate two-phonon γ bands built on 4^+ states are also observed in these nuclei. These bands show a similar trend to the γ bands of decreasing excitation energy. The nature of these collective excitations has been a controversial subject for several decades and is still a matter of debate.

A comprehensive Coulomb excitation study by Wu *et al.*, [16–18] measured both diagonal and off-diagonal matrix elements, including those of the 2^+ and the 4^+ γ bands in the even-even $^{186-192}$Os nuclei. The results suggested that the expectation values for their triaxiality parameter $\langle\cos 3\delta\rangle$ correspond to a pronounced nonaxiality of the nuclear shape for all measured bands, including the ground-state band, the γ band, and the 4^+ band. For axially symmetric prolate shape $\langle\cos 3\delta\rangle = 1$, for axially symmetric oblate shape $\langle\cos 3\delta\rangle = -1$, while for triaxial shape with $\gamma = 30°$, $\langle\cos 3\delta\rangle = 0$. The nonaxiality becomes larger for the heavier Os isotopes as the magnitude of the measured $\langle\cos 3\delta\rangle$ decreases, while the measured variance of the nonaxiality parameter, $\sigma(\cos 3\delta)$, shows values well below the characteristic values for harmonic γ vibrations but is consistent with a rigid triaxial shape. Furthermore, the nearly spin-independent values of $\langle Q^2\rangle$ for all bands suggest rotation-like rather than vibration-like excitation within the bands.

The experimental results in Refs. [16–18] were compared with several simple theoretical models and it was

TABLE I. The angular distribution ratios, R_{AD}, the γ-ray intensities and the polarization asymmetries A_P measured for the γ-ray transitions with energies of E_γ, together with the assigned multipolarities (γ Mult.). E_i (I_i^π) and E_f (I_f^π) are the energy (spins) for the initial and final levels, respectively. The star ($*$) symbols indicate the new transitions that have been established in the current work. Blanks refer to information that could not be obtained. The uncertainties on the γ-ray energies are typically of 0.3 keV for strong transitions and up to 0.5 keV for weak transitions and doublets.

E_i (keV)	E_f (keV)	E_γ (keV)	I_γ	I_i^π	I_f^π	R_{AD}	A_p	γ Mult.
				Band 1				
617.8	257.1	360.7	42.3(2)	$15/2^+$	$11/2^+$	0.71 (4)	0.04 (9)	$E2$
617.8	419.0	199.0	100.0(3)	$15/2^+$	$13/2^+$	0.41 (4)		$M1/E2$
1084.2	617.8	466.5	52.8(2)	$19/2^+$	$15/2^+$	0.82 (3)	0.01 (8)	$E2$
1084.2	818.4	265.9	20.7(2)	$19/2^+$	$17/2^+$	0.41 (7)		$M1/E2$
1647.3	1084.2	563.0*	27.7(2)	$23/2^+$	$19/2^+$	0.83 (2)	0.03 (12)	$E2$
1647.3	1287.0	360.5*	7.3(1)	$23/2^+$	$21/2^+$	0.33 (7)		$M1/E2$
2301.4	1647.3	654.1*	7.8(1)	$27/2^+$	$23/2^+$	0.91 (2)		$E2$
2301.4	1825.8	475.5*	2.9(2)	$27/2^+$	$25/2^+$	0.59 (8)		$M1/E2$
3032.3	2301.4	730.9*	2.8(2)	$31/2^+$	$27/2^+$	0.93 (3)		$E2$
3814.5	3032.3	782.2*	0.9(1)	$35/2^+$	$31/2^+$	0.77 (6)		$E2$
				Band 2				
419.0	257.1	161.9	131(20)	$13/2^+$	$11/2^+$	0.45 (1)		$M1/E2$
818.4	419.0	399.4	51.5(2)	$17/2^+$	$13/2^+$	0.89 (2)	0.20 (14)	$E2$
818.4	617.8	200.3	44.0(2)	$17/2^+$	$15/2^+$	0.45 (1)		$M1/E2$
1287.0	818.4	468.6*	42.8(2)	$21/2^+$	$17/2^+$	0.89 (1)	0.08 (11)	$E2$
1287.0	1084.2	202.6*	7.7(1)	$21/2^+$	$19/2^+$	0.38 (3)		$M1/E2$
1825.8	1287.0	538.8*	18.0(2)	$25/2^+$	$21/2^+$	0.94 (2)	0.02 (18)	$E2$
1825.8	1647.3	178.4*	2.4(1)	$25/2^+$	$23/2^+$	0.37 (2)		$M1/E2$
2442.9	1825.8	617.1*	9.9(1)	$29/2^+$	$25/2^+$	0.92 (2)	0.06 (20)	$E2$
3129.3	2442.9	686.4*	3.4(2)	$33/2^+$	$29/2^+$	0.98 (2)		$E2$
3854.1	3129.3	724.7*	1.2(2)	$37/2^+$	$33/2^+$	0.83 (7)		$E2$
4575.9	3854.1	721.8*	0.5(1)	$41/2^+$	$37/2^+$	0.73 (7)		$E2$
				Band 3				
894.2	257.1	637.1*	47.5(20)	$15/2^+$	$11/2^+$	0.74 (2)		$E2$
894.2	419.0	475.2*	31.3(11)	$15/2^+$	$13/2^+$	0.38 (2)		$M1/E2$
1381.3	894.2	487.1*	7.2(3)	$19/2^+$	$15/2^+$	0.77 (2)		$E2$
1381.3	818.4	562.7*	19.4(7)	$19/2^+$	$17/2^+$	0.40 (2)		$M1/E2$
1381.3	1126.5	254.8*	7.6(3)	$19/2^+$	$17/2^+$	0.54 (2)		$M1/E2$
1954.8	1381.3	573.5*	6.7(2)	$23/2^+$	$19/2^+$	0.73 (2)		$E2$
1954.8	1287.0	667.6*	4.0(2)	$23/2^+$	$21/2^+$	0.27 (4)		$M1/E2$
2592.8	1954.8	638.0*	2.2(2)	$27/2^+$	$23/2^+$	0.76 (2)		$E2$
2592.8	1825.8	767.0*	1.8(2)	$27/2^+$	$25/2^+$	0.41 (3)		$M1/E2$
3293.6	2592.8	700.8*	1.9(8)	$31/2^+$	$27/2^+$	0.92 (2)		$E2$
3293.6	2442.9	850.6*	1.2(2)	$31/2^+$	$29/2^+$			$M1/E2$
				Band 4				
1126.5	419.0	707.5*	20.6(7)	$17/2^+$	$13/2^+$	0.86 (2)		$E2$
1126.5	617.8	508.5*	44.8(14)	$17/2^+$	$15/2^+$	0.26 (2)		$M1/E2$
1126.5	894.2	232.2*	10.3(3)	$17/2^+$	$15/2^+$	0.34 (2)		$M1/E2$
1126.5	818.4	308.1*	5.1(2)	$17/2^+$	$17/2^+$	0.37 (2)		$M1/E2$
1646.5	818.4	828.2*	2.9(2)	$21/2^+$	$17/2^+$	0.77 (2)		$E2$
1646.5	1126.5	520.0*	8.0(3)	$21/2^+$	$17/2^+$	0.71 (4)		$E2$
1646.5	1287.0	(359.5)*	3.0(2)	$21/2^+$	$21/2^+$			$M1/E2$
1646.5	1381.3	265.4*	5.4(2)	$21/2^+$	$19/2^+$	0.35 (3)		$M1/E2$
2241.3	1646.5	594.8*	8.1(3)	$25/2^+$	$21/2^+$	0.74 (2)		$E2$
2241.3	1287.0	954.1*	1.0 (2)	$25/2^+$	$21/2^+$	0.93 (9)		$E2$
2936.8	2241.3	695.5*	3.0(2)	$29/2^+$	$25/2^+$	0.72 (5)		$E2$
2936.8	1825.8	(1110.8)*	0.6(1)	$29/2^+$	$25/2^+$			$E2$
3672.8	2936.8	(736.0)*	0.6(1)	$(33/2^+)$	$29/2^+$			$E2$

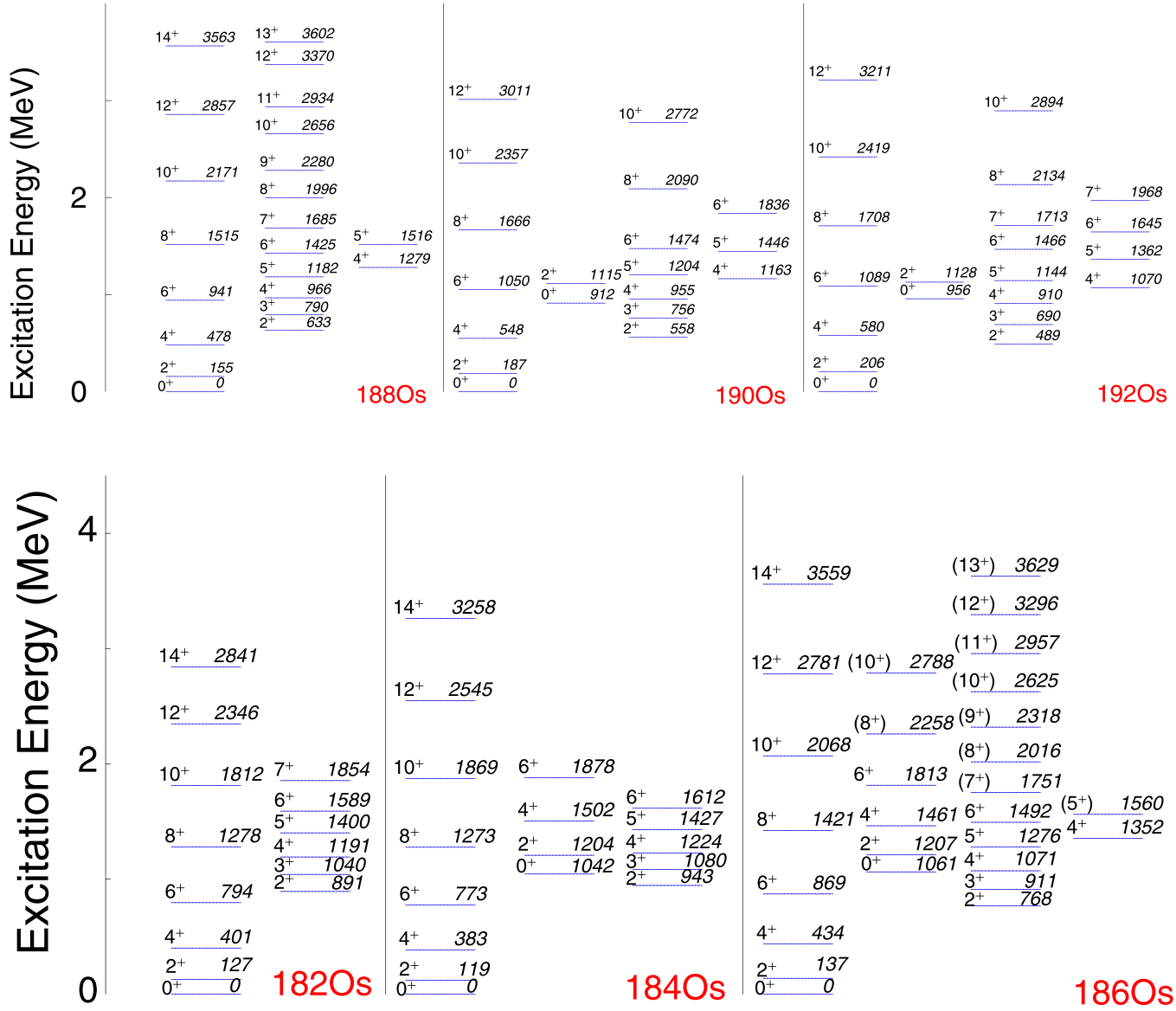

FIG. 2. Summary of collective excitations in the even-even stable osmium isotopes showing the ground state and the excited 0^+_2, 2^+, and 4^+ rotational bands [10–15].

concluded that none of the models could satisfactory reproduce the experimental data. Nevertheless, it was suggested that the models based on a γ-soft nuclear shape are more successful. In particular the 4^+ bands were suggested as probably produced by a two-phonon γ vibration. However, in a following paper it was pointed out that these conclusions did not consider previous results from transfer and inelastic scattering experiments [19]. The proton pick-up reaction ^{191}Ir(t, α) ^{190}Os [20] and the proton stripping reactions ^{185,187}Re(^{3}He, d) ^{186,188}Os [21] show that the 4^+ bands in the Os isotopes have a very strong component of 1p-1h proton configuration. They are also strongly populated in (p, p′) and (α, α') with L = 4 angular distributions [22–24], in particular the 4^+ state at 1163 keV in ^{190}Os is a mixed state with dominant 1p-1h and hexadecapole components, while the possible two-phonon γ-vibrational component is smaller.

Almond *et al.*, [25] have revisited the extensive Coulomb excitation data of [16] and re-analyzed it in terms of a triaxial rotor model with independent inertia and electric quadrupole tensors [26]. They concluded that the model gives an improved description of the large set of measured $E2$ matrix elements. The success of the model for the ground-state and the γ band were not considered as sufficient proof that the Os nuclei have a stable triaxial shape. It was pointed out that the discussion of whether the triaxial shape is stable or soft needs further experimental data. It should also be noted that the observation of the expected partner two-phonon $K = 0^+_{\gamma\gamma}$ band, that is part of the vibrational description of these nuclei, will be a strong argument in favour of dominating γ vibration, however, such bands are not yet observed.

In the present paper excited states in ^{187}Os were studied, as more information on the collective structure of the ^{186}Os core might be obtained by an investigation of the manner in

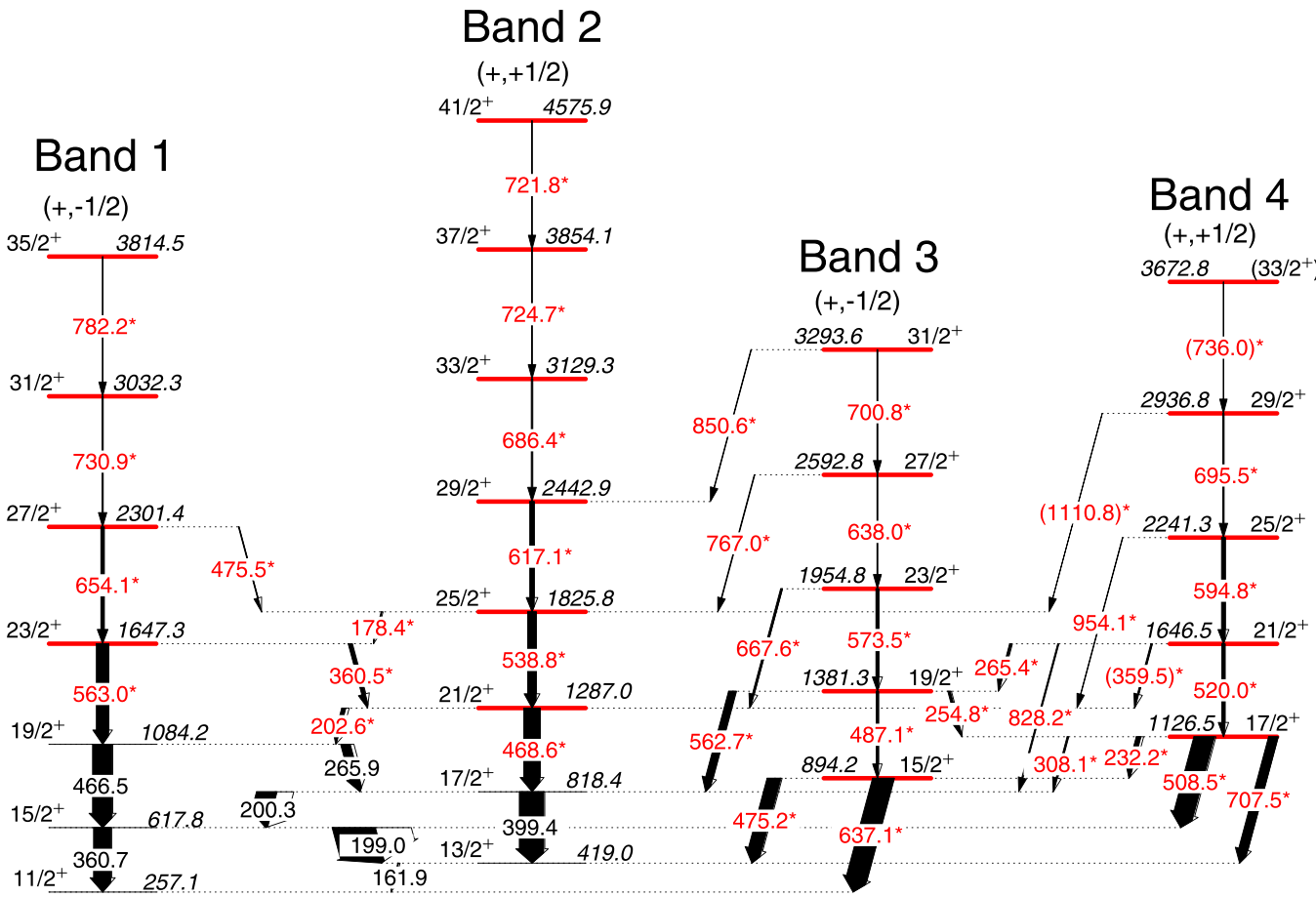

FIG. 3. Partial level scheme of ^{187}Os deduced from the current work showing the positive-parity bands. New transitions are labeled in red and asterisk (*) symbol while previously known transitions are labeled in black.

which the odd neutron couples to the core excitations. The collective excitations of the core lie within the pairing gap and therefore will couple with the odd neutron and produce rotational bands at a low excitation energy. For example, a single-particle orbital with an angular momentum j can couple to the one-phonon quadrupole vibrations of the core, either with its angular momentum j parallel to the vibrational angular momentum to produce $K_> = (2 + j)$, or it can be antiparallel to give a rotational band with $K_< = |2 - j|$. In the transitional region there are very few examples where both $K_>$ and $K_<$ couplings have been reported [27,28]. On the other hand, if the γ band involves a large single-particle component from the orbital j a blocking effect can occur. For instance the blocking observed in ^{155}Gd for the coupling of the $h_{11/2}$ neutron and the 0_2^+ state of the core, suggested that this core state corresponds to a wave function with a considerable $\nu h_{11/2}$ contribution [29].

In the current work we investigate the rotational bands of the even-odd ^{187}Os isotope, in particular the bands associated with the couplings of the $i_{13/2}$ neutron orbital with the ground-state and γ bands in the ^{186}Os core. Results pertaining to bands built on the negative-parity configurations in ^{187}Os have been published in Ref. [30].

II. EXPERIMENT AND DATA ANALYSIS

The AFRODITE γ-ray spectrometer [31] was used to detect $\gamma - \gamma$ coincidences produced using the ^{186}W(^{4}He, 3n)^{187}Os reaction at 37.0 MeV. The array consisted of 11 HPGe clover detectors in BGO shields. The ^{4}He beam was delivered by the $k = 200$ Separated Sector Cyclotron of iThemba LABS and impinged on a stack of four ^{186}W targets, mounted on thin carbon foils with a total thickness of 400 μg/cm^2. Events of coincident γ rays were recorded if the detection of two or more γ rays occurred within a 200 ns window. A total of about 2×10^9 coincidence events were sorted into a E_{γ_1}-E_{γ_2} matrix, which was used to extend the level scheme of ^{187}Os. Measured angular distribution ratios were used to assign spins to the excited nuclear states. The angular distribution ratios in this work are defined as

$$R_{AD} = \frac{I_{\gamma_1}^{135^\circ}}{I_{\gamma_1}^{90^\circ}}. \quad (3)$$

The numerator of Eq. (3) denotes the intensity of the γ ray of interest γ_1 detected at an angle of 135°, in coincidence with γ_2 detected in all detectors. The denominator of Eq. (3)

denotes the intensity of γ_1 detected at an angle of 90°, in coincidence with γ_2 detected in all detectors. All the R_{AD} ratios in Table I were obtained by setting a gate on pure stretched quadrupole transitions. For a gate set on a well-known stretched quadrupole transition, the R_{AD} ratio gives a value of 0.43 for a stretched dipole and a value of 0.87 for a stretched quadrupole transition.

The linear polarization asymmetries A_p have been used to determine the electromagnetic nature of the γ rays observed in this work. Here A_p is defined by

$$A_p = \frac{\alpha N_V - N_H}{\alpha N_V + N_H}, \tag{4}$$

where N_V and N_H are the number of γ rays scattered between the crystals of the clover detectors at 90° perpendicular and parallel to the beam direction, respectively. The relative efficiency parameter $\alpha = N_H/N_V$, is determined using unpolarized γ rays. For polarization measurements the A_p values yield $A_p < 0$ and $A_p > 0$ for stretched magnetic and electric transitions, respectively.

III. EXPERIMENTAL RESULTS

The nuclear structure of ^{187}Os was previously investigated in Refs. [32–41]; in these works the band heads and some low-energy levels of the rotational bands of ^{187}Os were observed. This paper presents new experimental data on positive-parity bands of ^{187}Os, as shown in Fig. 3.

The previously observed positive-parity bands, as reported by Sodan *et al.*, [40], were confirmed and extended to higher spins, see bands 1 and 2 in Fig. 3. These bands are signature partner bands built on an isomeric state at 257.1 keV with a half-life of 231 μs [40]. Evidence for the presence of this isomeric state was first reported by Colon [42], who deduced that a 156.7-keV $M2$ transition with $T_{1/2} = 231$ μs belongs to ^{187}Os, but was not able to place it in the decay scheme. The 156.7-keV $M2$ transition was then placed in the ^{187}Os decay scheme by Malmskog *et al.*, [41], who concluded that this transition directly feeds the 100.5-keV level leading to the establishment of the 257.1-keV isomeric state. Bands 1 and 2 have been previously observed up to $I^\pi = 19/2^+$ and $17/2^+$, respectively [40].

The present work extended bands 1 and 2 up to $I^\pi = 35/2^+$ and $41/2^+$, respectively, see Fig. 3. To illustrate the transitions in bands 1 and 2, gated spectra are shown in Figs. 4 and 5. The combined results of the R_{AD} and polarization measurements, performed for the in-band members of bands 1 and 2, are consistent with them having stretched $E2$ character. The R_{AD} ratios were also obtained for some of the interlinking transitions between these bands, and are consistent with stretched dipole nature, see Table I.

Bands 3 and 4 are new bands built on the 894.2-keV level. The transitions were grouped together following their coincidence relationships and γ-ray intensities. The measured angular distribution ratios of these transitions support the proposed spins, providing evidence on the $E2$ nature of the in-band transitions. As shown in Fig. 3, bands 3 and 4 decay predominantly to band 2, which is the yrast positive-parity band. Bands 3 and 4 are linked with stretched dipole transitions, suggesting that these bands are signature partners. To illustrate the transitions associated with these bands, a few gated spectra are shown in Figs. 6 and 7.

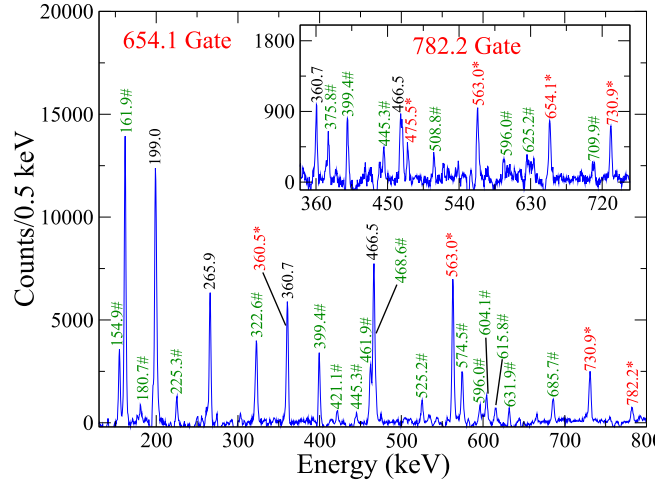

FIG. 4. Coincidence spectrum obtained by setting a gate on the 654.1-keV transition of band 1. New transitions are labeled in red and asterisk (*), while contaminants and other transitions of ^{187}Os not associated with the band of interest are denoted by green and hash (#) symbol. The known transitions associated with the band of interest are labeled in black. The spectrum gated on 782.2 keV is inserted to show the 475.5- and 654.1-keV transitions.

The spin and parity of the new 894.2-keV level, the band head of band 3, are established by the measured stretched dipole and stretched quadrupole nature of the 475.2- and 637.1-keV transitions, respectively, see Table I. The spin assignment of this band is further confirmed by the measured

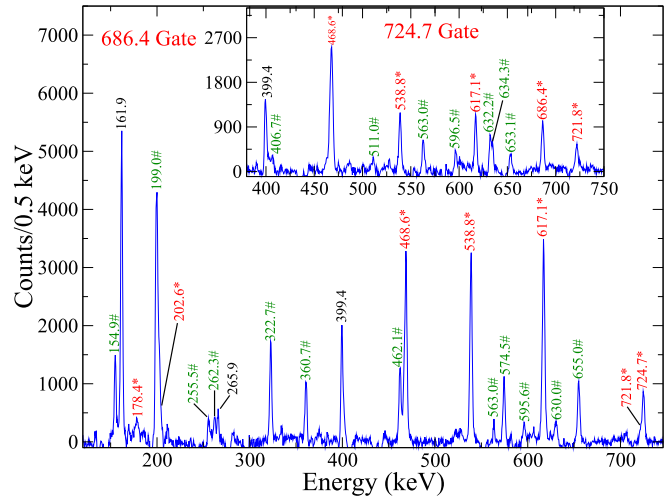

FIG. 5. Coincidence spectrum obtained by setting a gate on the 686.4-keV transition of band 2. New transitions are labeled in red and asterisk (*), while contaminants and other transitions of ^{187}Os not associated with the band of interest are denoted by green and hash (#) symbol. The known transitions associated with the band of interest are labeled in black. The spectrum gated on 724.7 keV is inserted to show the 686.4-keV transition.

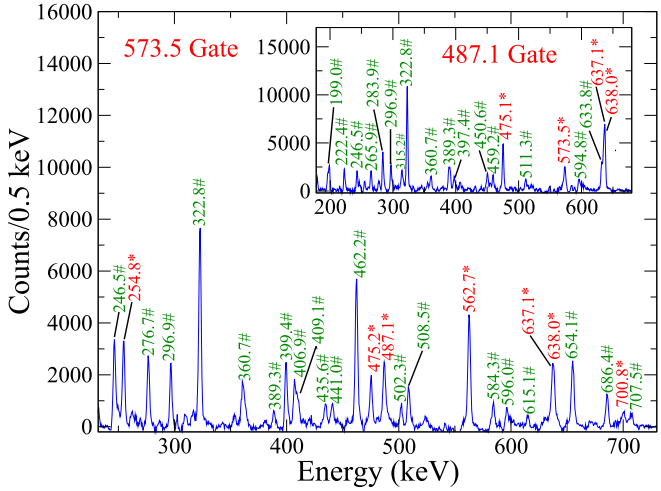

FIG. 6. Coincidence spectrum obtained by setting a gate on the 573.5-keV transition of band 3. New transitions are labeled in red and asterisk (*), while contaminants and other transitions of ^{187}Os not associated with the band of interest are denoted by green and hash (#) symbol. The spectrum gated on 487.1 keV is inserted to show the 573.5-keV transition.

stretched dipole nature of the transitions linking bands 3 and 2.

The spin of the 1126.5-keV level, the band head of band 4, is established by the angular distribution ratios of the 508.5- and 707.5-keV transitions, which suggest stretched dipole and quadrupole nature, respectively, see Table I. Band 4 decays to band 3 via the 232.2- and 265.4-keV transitions, which are stretched dipole in nature. Band 4 decays to band 2 mostly through high-energy ($E > 800$-keV) stretched quadrupole transitions. The only unstretched dipole transition observed to link these bands is the 308.1-keV transition. Its R_{AD} value is

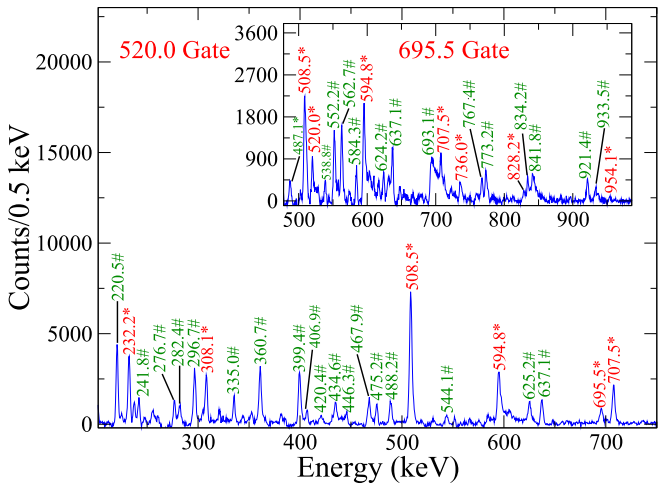

FIG. 7. Coincidence spectrum obtained by setting a gate on the 520.0-keV transition of band 4. New transitions are labeled in red and asterisk (*), while contaminants and other transitions of ^{187}Os not associated with the band of interest are denoted by green and hash (#) symbol. The spectrum gated on 695.5 keV is inserted to show the 520.0-, 736.0-, 828.2-, and 954.1-keV transitions.

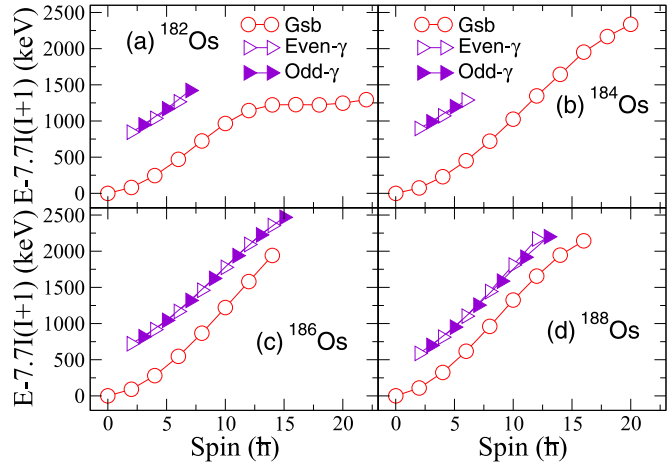

FIG. 8. Compilation of the experimental excitation energies with respect to a rigid rotor reference for the ground state bands and the γ bands of ^{182}Os [10], ^{184}Os [11], ^{186}Os [12] and ^{188}Os [13]. The even- and odd-spin sequences of the γ bands are labeled with open and closed symbols, respectively, and the same colours.

too low to be a pure dipole, therefore this transition probably has mixed $M1 + E2$ nature. One transition with energy of 254.8 keV links band 3 to band 4 and was measured as a stretched dipole in agreement with the proposed spin assignments.

IV. DISCUSSION

In this paper bands 1 and 2 were extended and two new positive-parity bands, bands 3 and 4, were identified. Bands 1 and 2 have been previously assigned as signature partner bands where the odd neutron occupies the nearest to the Fermi level $i_{13/2}$ orbital [40]. The band-head level of band 3 has an excitation energy of 894.2 keV, which is too low for a 3-quasiparticle configuration. Therefore in a quest to identify its microscopic nature, we consider the possible couplings of the odd $i_{13/2}$ neutron with the excited collective states of the core. As illustrated in Fig. 2, the lowest collective excitation in the even-even Os isotopes is the γ band. The excitation energies of the ground-state and the γ bands in the even-even $^{182-188}$Os isotopes with respect to a rigid-rotor reference are shown in Fig. 8. As mentioned earlier the excitation energies of the γ band decrease for the heavier isotopes. Figure 9 shows a similar plot for the excitation energies of the positive-parity bands in ^{187}Os in comparison with the excitation energies of the corresponding bands in ^{183,185}Os. The Fermi level for neutrons for these Os isotopes lies at the upper part of the $i_{13/2}$ subshell near the 9/2[624] and 11/2[615] Nilsson orbitals. The lowest-energy positive-parity band in ^{183}Os is built above a $9/2^+$ state and was associated with the 9/2[624] Nilsson orbital [43]. In ^{185}Os positive-parity bands associated with both the 9/2[624] and 11/2[615] Nilsson orbitals were observed with the latter lying at lower energy [44]. In ^{187}Os the yrast positive-parity band is based on a $11/2^+$ level and thus the band was associated with the 11/2[615] Nilsson orbital. The change can be explained as due to the raising of the Fermi level within the $i_{13/2}$ subshell for the heavier Os

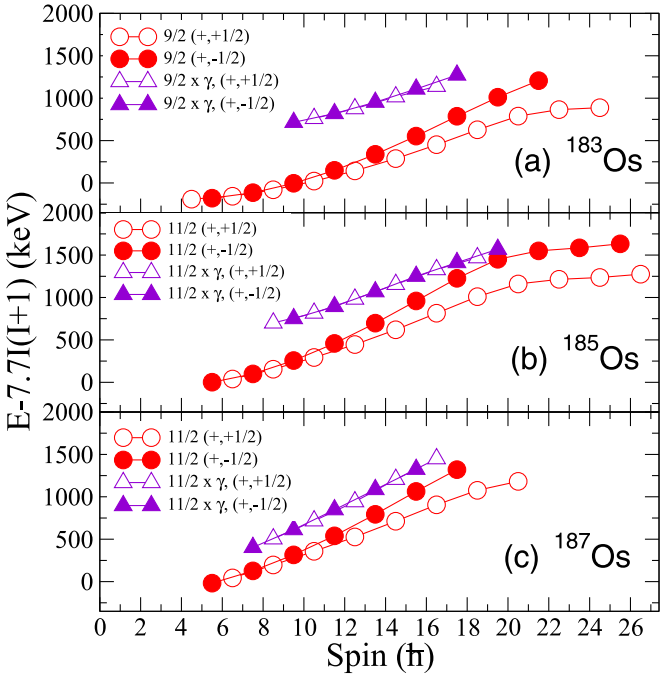

FIG. 9. Experimental excitation energies relative to a rigid rotor reference for the positive-parity bands in ^{187}Os in comparison with the corresponding bands in ^{183}Os [43] and ^{185}Os [44]. The signature partner bands are labeled in the same colours. Open symbols denote positive signature and closed symbols represent negative signature.

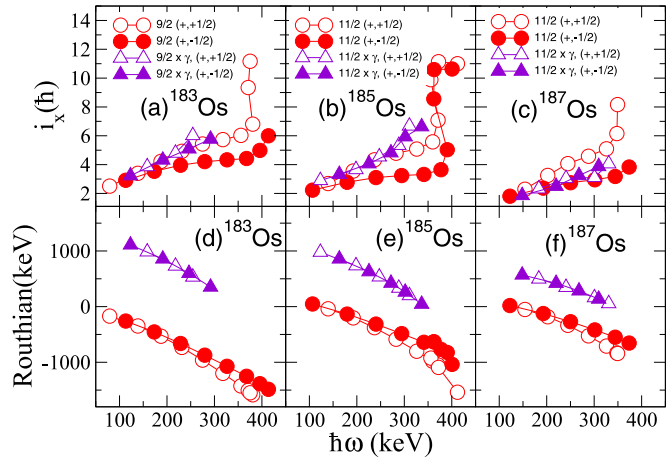

FIG. 10. Alignment and Routhian plots of the bands in ^{187}Os in comparison with those in the ^{183}Os and ^{185}Os isotopes. Harris parameters used here are: $J_0 = 24\,\hbar^2$ MeV^{-1} and $J_1 = 66\,\hbar^4$ MeV^{-3} [44]. The yrast positive-parity bands are labeled by the band spin, while the excited bands are labeled as a coupling with the γ band. The signature partner bands are labeled in the same colours, open symbols denote the positive signature and closed symbols represent the negative signature sequences.

isotopes. These assignments assume that the nuclear shape is axially symmetric, and thus the projection of the total angular momentum, K, and the single-particle angular momentum Ω, on the long axis are conserved, and $K = \Omega$. The distinct resemblance of the excited positive-parity bands in ^{183,185}Os with the γ bands in ^{182,184}Os was noted and these bands were interpreted as a coupling of the $i_{13/2}$ yrast band with the γ band of the core, [43,44].

For nuclei with axially symmetric shape the γ band corresponds to a $K = 2^+$ γ vibration, thus the coupling with a Nilsson state with projection Ω can produce excited bands with $K_> = \Omega + 2$ and $K_< = \Omega - 2$. The excited positive-parity bands in ^{183,185}Os were interpreted as a coupling with the core to give $K_>$ [43,44]. The new bands in ^{187}Os, bands 3 and 4, follow a similar trend of the excitation energies, see Fig. 9, as the corresponding bands in ^{183,185}Os, thus we propose that they result from a coupling with the γ band. Such assignment is further supported by the observed trend of decreasing excitation energy of the excited positive-parity bands for the heavier Os isotopes, which is very similar to the decreasing energy trend observed for the γ bands in the corresponding cores, see Fig, 8. In addition bands 3 and 4 decay only to the levels of bands 1 and 2, which also supports the proposed interpretation. Fig. 10 shows the experimental alignments and Routhians for the positive-parity bands in ^{187}Os in comparison with the corresponding bands in the neighboring ^{183,185}Os isotopes. They are calculated assuming $K = 9/2$ and $K = 13/2$ for the yrast (shown with circles) and the excited (shown with triangles) bands in ^{183}Os, respectively, while $K = 11/2$ and $K = 15/2$ were used for these bands in ^{185,187}Os. The plots highlight the similarities of the bands in the three Os isotopes. Following all presented comparisons, the new bands 3 and 4 are associated with a coupling with the γ band of the even-even core.

The yrast positive-parity band, (bands 1 and 2 in Fig. 3), shows a large signature splitting. In principle a single-particle configuration with a large projection Ω on the symmetry axis, such as $\Omega = 11/2$, is not expected to show signature splitting. Similar splitting was observed in the ^{183,185}Os neighbours, but was not discussed. It should also be noted that while the splitting is present for the yrast bands in ^{183,185,187}Os, it is absent for the excited bands, see Fig. 9. To study the signature splitting cranked shell model (CSM) calculations were carried out, see Fig. 11. The same parameters as used for ^{186}Os, [45] were employed, with quadrupole deformation $\varepsilon_2 = 0.198$, hexadecapole deformation $\varepsilon_4 = 0.054$, pairing gap $\Delta = 0.647$ MeV, triaxial deformation of $\gamma = 0°$, while the Fermi level was increased to $\lambda = 53.4$ MeV to account for the additional neutron. As expected, the Routhians corresponding to the high-Ω configurations such as $11/2[615]$ and $9/2[624]$ do not show signature splitting. However the down-sloping Routhian originating from the $1/2[651]$ orbital from the $g_{9/2}$ subshell interacts strongly with the positive-signature Routhians and pushes them down, creating signature splitting. Therefore signature splitting where the $\alpha = +1/2$ Routhian becomes favoured is predicted by the calculations in agreement with the experimentally observed phase of the signature splitting. On the other hand, the experimental data show signature splitting throughout the whole spin range of the yrast band, while the CSM calculations suggest splitting for rotational frequency above 0.35 MeV (for the lowest-energy Routhian). This indicates that the origin of the signature splitting is most probably

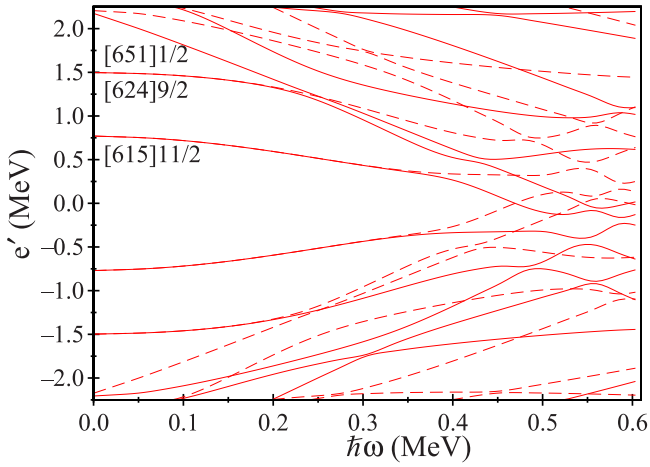

FIG. 11. Cranked shell model positive-parity Routhians for ^{186}Os with N = 110 as a function of the rotational frequency, $\hbar\omega$. In this figure, solid lines represent quasiparticle trajectories with signature $\alpha = +1/2$ and dashed lines are used for quasiparticle trajectories with signature $\alpha = -1/2$.

of different nature, for instance it can be caused by triaxiality of the nuclear shape.

In the neighboring Os nuclei the nuclear shape was assumed to be axially symmetric. An assumption of near axially symmetric shape might be suitable for ^{187}Os as well, however the decreasing trend of the excitation energy of the γ bands with mass, see Fig. 2, indicates a more significant role for the γ degree of freedom, where triaxial rigidity might occur.

Calculations within the cranked Nilsson-Strutinsky-Bogoliubov (CNSB) model (see Refs. [46–48]) were carried out using standard parameters for the Nilsson potential [49]. Within these calculations the nucleon configurations are labeled with their parity π and signature α as (π, α). The potential energy surface (PES) for the yrast $(+,+1/2)$ configuration was plotted in Fig. 13 of Ref. [30]. The energy surface shows a minimum near $\varepsilon_2 \approx 0.2$ and $\gamma \approx -8^\circ$ for I $\approx$ 6.5. This minimum shifts to a larger triaxiality with $\gamma = -17^\circ$ at I $\approx$12.5 and becomes stiffer. This suggests that the shape of ^{187}Os develops a stable triaxial deformation. The observed minima suggest rotation around the intermediate axis.

To study further the features of the rotational bands for a deformed triaxial shape we carried out quasiparticle-plus-triaxial-rotor (QTR) model calculations. The QTR model uses a modified oscillator potential with standard parameters [49] and standard pairing interaction [50]. The deformation parameters were quadrupole deformation of $\varepsilon_2 = 0.21$, hexadecapole deformation of $\varepsilon_4 = 0$, and triaxial deformation of $\gamma = 21^\circ$, while the γ dependence of the moments of inertia was described by the irrotational-flow model. The spin dependence of the moments of inertia were described by Harris parameter of $J_0 = 18.5\ \hbar^2\ \text{MeV}^{-1}$ and $J_0 = 62.5\ \hbar^4\text{MeV}^{-3}$. The seven positive-parity orbitals (#25 to #31) that were found near the neutron Fermi level and included in the calculations are listed in Table II.

In QTR the single-particle orbitals are superpositions of the spherical shell-model basis functions. These basis wave functions are labeled with the spherical-shell labels and also with the projection of the single-particle angular momentum along the long nuclear axis, Ω_ℓ, see Table II. Each single-particle orbital reflects a superposition of a number of basis wave functions with their corresponding probabilities. As shown in the table, most of the positive-parity single-particle orbitals near the Fermi level correspond to major contributions from the $i_{13/2}$ subshell. Since the shape is triaxial the orbitals may have contributions from basis wave functions with different values of Ω_ℓ. Orbital #27 was found closest to the Fermi level, and it is almost entirely of $i_{13/2}$ nature with angular momentum projection on the long axis of $\Omega_\ell = 9/2$.

The model couples single-particle and rotational degrees of freedom and calculates the excitation energies and wave functions for the states of the predicted rotational bands. Figure 12 shows a comparison of the calculated excitation energies of the two lowest-energy positive-parity bands with the experimental data. The excitation energies for both bands are reproduced well by the model. It is noticeable that while the QTR model predicts signature splitting for the yrast band with the same phase as in the experimental data, it has smaller amplitude.

To understand better the nature of the QTR bands the calculated wave functions were examined. In general, the rotational bands predicted by the QTR model involve two types of excitations, single-particle (where the wave function comprises a major component from another single-particle orbital)

TABLE II. Composition of the 7 positive-parity orbitals near the neutron Fermi surface, which were found to contribute to the levels of the calculated positive-parity bands of ^{187}Os. The orbitals are described as a superposition of spherical shell-model wave function, labeled by the corresponding spherical subshell, e.g., $i_{13/2}$, and the projection of the single-particle angular momentum on the long axis Ω_ℓ. The basis wave functions with contributions larger than 5%, are listed for each orbital included in the calculations.

Orbital	Contributions by spherical shell-model basis functions
#25	73%($i_{13/2}$, 5/2), 10%($i_{13/2}$, 1/2), 6%($g_{9/2}$, 5/2)
#26	88%($i_{13/2}$, 7/2)
#27	94%($i_{13/2}$, 9/2)
#28	33%($i_{13/2}$, 11/2), 28%($g_{9/2}$, 1/2), 14%($d_{5/2}$, 1/2), 8%($i_{13/2}$,1/2), 6%($g_{9/2}$, 3/2)
#29	63%($i_{13/2}$, 11/2), 15%($g_{9/2}$, 1/2), 8%($d_{5/2}$, 1/2)
#30	31%($g_{9/2}$, 3/2), 17%($i_{11/2}$, 1/2), 10%($g_{7/2}$, 1/2), 9%($i_{11/2}$, 3/2), 8%($i_{13/2}$, 3/2), 8%($d_{5/2}$, 3/2)
#31	97%($i_{13/2}$, 13/2)

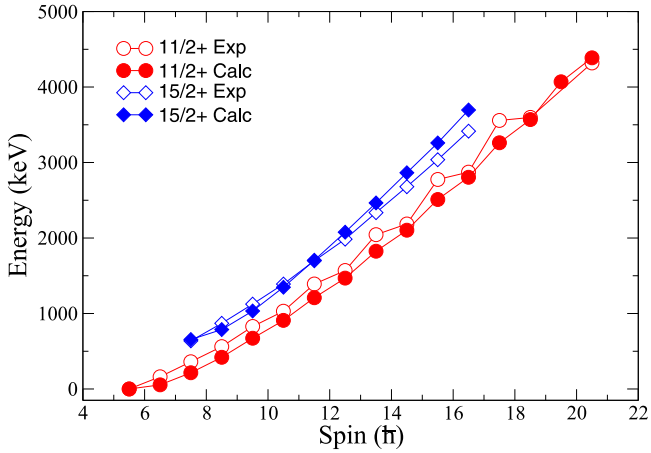

FIG. 12. Calculated excitation energies for the two lowest-energy positive-parity bands of ^{187}Os in comparison with experimental data.

and collective (where the wave function comprises different rotational component). In general, the bands calculated within QTR correspond to 3D rotation and represent a precession of the total angular momentum along a given axis. Such bands have been called tilted precession (TiP) bands [51].

Figure 13 illustrates schematically the nature of the collective excitations at low rotational frequency assuming that the single-particle component of the wave functions remains unchanged and has a dominant contribution from the orbital with projection $\Omega_\ell = 11/2$. A triaxial nucleus with irrotational-flow moments of inertia prefers to rotate around its intermediate axis because this moment of inertia is largest, thus the rotation has lowest energy for given rotational angular momentum. The yrast band, shown in blue in Fig. 13, corresponds to such favoured rotation, where the nucleus rotates around its intermediate axis, while the single-particle angular momentum remains aligned along the long nuclear axis. The excited band, shown in red in Fig. 13, corresponds to the same coupling, however, it also involves one unit of unfavoured rotation, which is $2\hbar$ along the long axis. The two bands were labeled by the $[\Omega_\ell, K_\ell]$ as $[11/2, 11/2]$ and $[11/2, 15/2]$, respectively. One should keep in mind that the sketch shown in Fig. 13 is simplified.

The wave functions for the yrast (TiP1) and excited (TiP2) bands in ^{187}Os combine different single-particle and collective contributions and are plotted in Figs. 14 and 15. The $11/2$ state from the yrast band, see Fig. 14, has about 56% contribution from a coupling of orbital #27 with rotation producing $K_\ell = 9/2$, see the column in sky blue. As listed in Table II, orbital #27 is dominated by $\Omega_\ell = 9/2$. Therefore the largest component of the wave function is from $\Omega_\ell = K_\ell = 9/2$, of the type $[9/2, 9/2]$. There are also two significant contributions from orbitals #28 and #29 and with $K_\ell = 11/2$, shown as yellow columns, which correspond to a $[11/2, 11/2]$ component. The purple column corresponds to orbital #26 and K = 7/2, therefore to a $[7/2, 7/2]$ component.

The $13/2$ state of the yrast TiP1 band has largest, about 50%, contribution from the $[9/2, 9/2]$ component (column shown in sky blue) and smaller contributions from $[11/2, 11/2]$ (the two columns in yellow) and $[7/2, 7/2]$ (the column shown in purple) components. As we approach higher-spin states of this band the contributions associated with orbitals #27, #28, and #29 decrease steadily, while those associated with orbital #26 increase. Such a trend suggests changes in the single-particle component favoring contributions with smaller projections on the long axis. Such a change is understood as induced by Coriolis realignment of the angular momentum of the odd neutron away from the long axis and towards the intermediate axis, which is the axis with largest moment of inertia. Therefore the yrast band in ^{187}Os is associated with a major contribution from the $[\Omega_\ell, K_\ell] = [9/2, 9/2]$ component at low spin, but at high spins Coriolis realignment of the single-particle angular momentum is also observed. It should be noted that the calculations find the head of this band at $I = 11/2$ and not $I = 9/2$, although the largest single-particle configuration is with $\Omega_\ell = 9/2$. For an axially symmetric

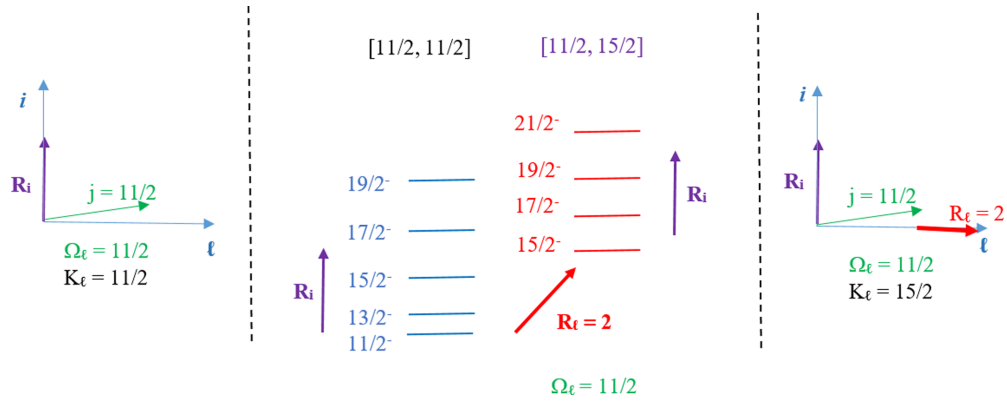

FIG. 13. Sketch illustrating the nature of the collective excitation in QTR model. Both bands illustrated in the middle panel are based on the same single-particle configuration with projection of the angular momentum along the long axis of $\Omega_\ell = 11/2$. The angular momenta coupling for the yrast and excited bands are shown in the left and right panels, respectively. The angular momentum in the yrast band increases due to favorite rotation around the intermediate axis, and the projection of the total angular momentum along the long axis is $K_\ell = \Omega_\ell = 11/2$. The angular momentum in the excited band includes one unit, $2\hbar$, of unfavoured rotation around the long axis, while the remaining rotation is around the intermediate axis, thus $K_\ell = \Omega_\ell + 2 = 15/2$. The bands are labeled according to $[\Omega_\ell, K_\ell]$.

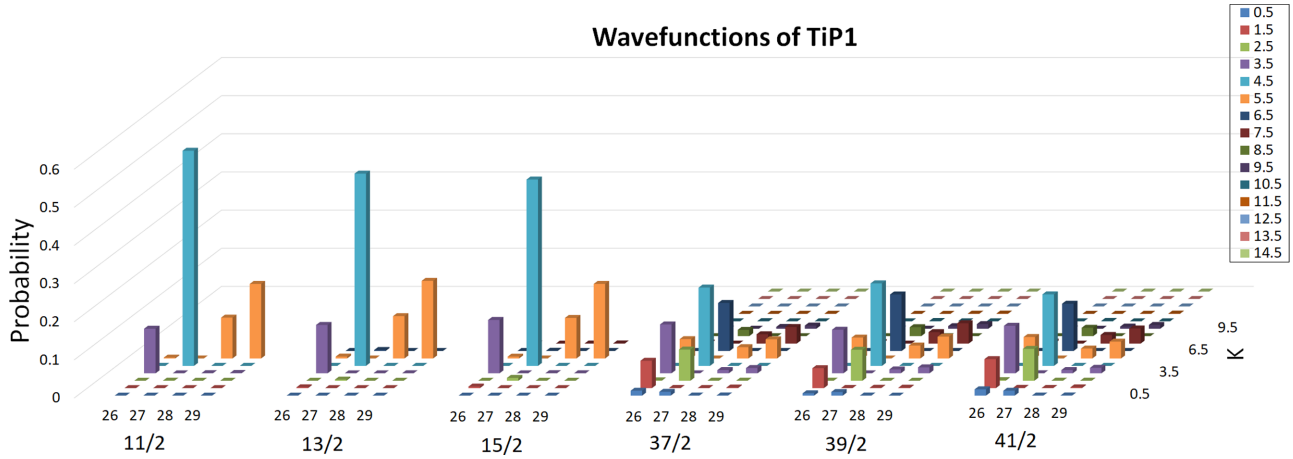

FIG. 14. Contributions of the wave functions labeled with their single-particle orbitals and projections K_ℓ on the long axis for the states with $I = 11/2$–$15/2$ and $37/2$–$41/2$ from the yrast, TiP1, band in ^{187}Os. The orbitals that contribute to the wave function, (26, 27, 28, and 29), are labeled on the x axis as in Table II. The corresponding K_ℓ values are shown on the y-axis and also illustrated with different colours, see the legend.

nucleus the band head spin of a strongly coupled band has $I = K = \Omega$. This, however, does not necessarily hold true for triaxial shape. In the present case, the QTR model found the lowest-energy $9/2^+$ state at 121.7 keV above the yrast $11/2^+$ state.

The wave functions for the states from the excited band, TiP2, are illustrated in Fig. 15. There is a major contribution from a coupling of orbital #27 with $K_\ell = 13/2$. This [9/2, 13/2] component suggests that there is $2\hbar$ rotation along the long axis, as illustrated in Fig. 13 for the excited band (shown in red). The 15/2 state has almost 53% contribution from this [9/2, 13/2] component, as shown by the column in navy blue. The contributions from orbitals #28 and #29, shown in dark red, correspond to components with [11/2, 15/2], while the column in yellow represents a [7/2, 11/2] component. Note the similarity in the single-particle component of this state with the wave function of the 11/2 state of TiP1 and the added rotational angular momentum of $2\hbar$ along the long axis.

At higher spins the states of TiP2 still have their largest contribution from the [9/2, 13/2] component, but represent a complex mixture of contributions with different nature, in particular there is an increase in the contributions associated with orbital #26, which represents Coriolis realignment of the odd neutron away from the long axis.

The QTR calculations successfully describe the observed bands in ^{187}Os. This does not prove that the nuclear shape has stable triaxial deformation, because one needs to also investigate an alternative description based on small vibrations of γ-soft nuclear shape. However, one can study the possible rigidity or softness of the nuclear shape if more detailed experimental data become available. For instance, the projection of the total angular momentum on the symmetry axis is a good quantum number for a nucleus with an axially symmetric γ-soft shape. The yrast and the γ bands in such even-even nuclei correspond to $K = 0$ and $K = 2$. Similarly in odd-mass nuclei the excited and the yrast bands correspond to $\Delta K = 2$. Therefore, the transitions linking the excited and the yrast bands should carry angular momentum of at least $2\hbar$. This indicates that the $\Delta I = 1$ and $\Delta I = 0$ linking transitions should be pure quadrupoles. This is different from the results from

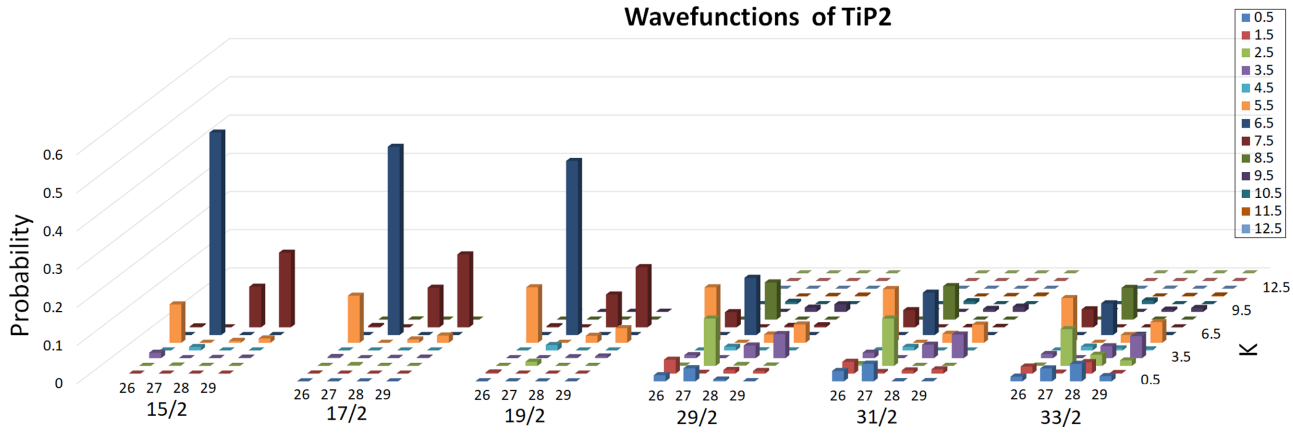

FIG. 15. The same as Fig. 14, but for TiP2 band.

the QTR model, where K is not conserved, thus the linking transitions have typically mixed $M1 + E2$ nature. Our data did not have sufficient statistics to measure linear polarization or enough angles to determine precisely the mixing ratios for the linking transitions.

V. CONCLUSION

The collective positive-parity states in ^{187}Os based on the $i_{13/2}$ configuration were investigated using the AFRODITE array. Our work has extended bands 1 and 2 and established two new bands, bands 3 and 4. The angular distribution ratios and linear polarization measurements have been used to assign spin and parity to the observed rotational bands. Based on comparison with the neighboring isotopes it was concluded that the new bands represent a coupling with the γ band of the even-even core. The quasiparticle-plus-triaxial-rotor model calculations provide a very good agreement with the experimental data. In order to distinguish between the possible interpretations based on a stable triaxial shape and on γ vibrations of an axially symmetric shape, measurements of the mixing ratios of the transitions decaying out of the excited band are needed. Our experimental setup did not have the geometry neither did the data have sufficient statistics to determine precisely these mixing ratios, however such measurements will be possible with the upgraded AFRODITE array in the future.

ACKNOWLEDGMENTS

It is a genuine pleasure to express our deep sense of gratitude to the iThemba LABS accelerator group for the beam. We thank John Simpson and the STFC Daresbury Laboratory for supplying the ^{186}W targets. Support for this work was provided by the National Research Foundation (NRF) of South Africa under Grants No. 90741, No. 95606, No. 109711, and No. 109134.

[1] J. M. Allmod and J. L. Wood, Phys. Lett. B **767**, 226 (2017).
[2] G. L. Zimba, S. P. Bvumbi, L. P. Masiteng, P. Jones, J. F. Sharpey-Schafer, S. N. T. Majola, T. S. Dinoko, O. Shirinda, J. J. Lawrie, J. E. Easton, N. A. Khumalo, L. Msebi, P. I. Mashita, P. Papka, D. G. Roux, and D. Negi, Eur. Phys. J. A **54**, 59 (2018).
[3] S. N. T. Majola, Z. Shi, B. Y. Song, Z. P. Li, S. Q. Zhang, R. A. Bark, J. F. Sharpey-Schafer, D. G. Aschman, S. P. Bvumbi, T. D. Bucher, D. M. Cullen, T. S. Dinoko, J. E. Easton, N. Erasmus, P. T. Greenlees, D. J. Hartley, J. Hirvonen, A. Korichi, U. Jakobsson, P. Jones *et al.*, Phys. Rev. C **100**, 044324 (2019).
[4] S. N. T. Majola, D. J. Hartley, L. L. Riedinger, J. F. Sharpey-Schafer, J. M. Allmond, C. Beausang, M. P. Carpenter, C. J. Chiara, N. Cooper, D. Curien, B. J. P. Gall, P. E. Garrett, R. V. F. Janssens, F. G. Kondev, W. D. Kulp, T. Lauritsen, E. A. McCutchan, D. Miller, J. Piot, N. Redon *et al.*, Phys. Rev. C **91**, 034330 (2015).
[5] S. N. T. Majola, M. A. Sithole, L. Mdletshe, D. Hartley, J. Timár, B. M. Nyakó, J. M. Allmond, R. A. Bark, C. Beausang, L. Bianco, T. D. Bucher, S. P. Bvumbi, M. P. Carpenter, C. J. Chiara, N. Cooper, D. M. Cullen, D. Curien T. S. Dinoko, B. J. P. Gall, P. E. Garrett *et al.*, Phys. Rev. C **101**, 044312 (2020).
[6] L. Mdletshe, S. S. Ntshangase, J. F. Sharpey-Schafer, S. N. T. Majola, T. R. S. Dinoko, N. A. Khumalo, E. A. Lawrie, R. A. Bark, T. D. Bucher, N. Erasmus *et al.*, Eur. Phys. J. A **54**, 176 (2018).
[7] J. F. Sharpey-Schafer, R. A. Bark, S. P. Bvumbi, T. R. S. Dinoko, and S. M. T. Majola, Eur. Phys. J. A **55**, 15 (2019).
[8] S. Jehangir, G. H. Bhat, J. A. Sheikh, S. Frauendorf, S. N. T. Majola, P. A. Ganai, and J. F. Sharpey-Schafer, Phys. Rev. C **97**, 014310 (2018).
[9] J. Ollier, J. Simpson, M. A. Riley, E. S. Paul, X. Wang, A. Aguilar, M. P. Carpenter, I. G. Darby, D. J. Hartley, R. V. F. Janssens, F. G. Kondev, T. Lauritsen, P. J. Nolan, M. Petri, J. M. Rees, S. V. Rigby, C. Teal, J. Thomson, C. Unsworth, S. Zhu, A. Kardan *et al.*, Phys. Rev. C **83**, 044309 (2011).
[10] C. Fahlander and G. D. Dracoulis, Nucl. Phys. A **375**, 263 (1982).
[11] C. Wheldon, G. D. Dracoulis, R. T. Newman, P. M. Walker, C. J. Pearson, A. P. Byrne, A. M. Baxter, S. Bayer, T. Kibédi, T. R. McGoram, S. M. Mullins, and F. R. Xu, Nucl. Phys. A **699**, 415 (2002).
[12] C. Wheldon, P. M. Walker, P. H. Regan, T. Saitoh, N. Hashimoto, G. Sletten, and F. R. Xu, Nucl. Phys. A **652**, 103 (1999).
[13] V. Modamio, A. Jungclaus, Z. Podolyak, Y. Shi, F. R. Xu, A. Algora, D. Bazzacco, D. Escrig, L. M. Fraile, S. Lenzi, N. Marginean, T. Martinez, D. R. Napoli, R. Schwengner, and C. A. Ur, Phys. Rev. C **79**, 024310 (2009).
[14] M. A. Cardona, D. Hojman, B. Roussière, J. Libert, J. Genevey, J. Sauvage, and The ISOCELE and ISOLDE Collaborations, Eur. Phys. J. A **31**, 141 (2007).
[15] M. Oshima, T. Morikawa, H. Kusakari, N. Kobayashi, M. Sugawara, Y. H. Zhang, A. Ferragut, S. Ichikawa, N. Shinohara, Y. Nagame, M. Shibata, Y. Gono, and T. Inamura, Nucl. Phys. A **557**, 635 (1993).
[16] C. Wu, D. Cline, T. Czosnyka, A. Backlin, C. Baktash, R. Diamond, G. Dracoulis, L. Hasselgren, H. Kluge, B. Kotlinski, J. Leigh, J. Newton, W. Phillips, S. Sie, J. Srebrny, and F. Stephens, Nucl. Phys. A **607**, 178 (1996).
[17] C. Y. Wu and D. Cline, Phys. Lett. B **382**, 214 (1996).
[18] C. Y. Wu, D. Cline, A. B. Hayes, M. W. Simon, R. Krücken, J. R. Cooper, C. J. Barton, C. W. Beausang, C. Bialik, M. A. Caprio, R. F. Casten, A. A. Hecht, H. Newman, J. Novak, N. Pietralla, K. Zyromski, and N. V. Zamfir, Phys. Rev. C **64**, 014307 (2001).
[19] D. G. Burke, Phys. Lett. B **406**, 200 (1997).
[20] R. D. Bagnell, Y. Tanaka, R. K. Sheline, D. G. Burke, and J. D. Sherman, Phys. Rev. C **20**, 42 (1979).
[21] A. A. Phillips, P. E. Garrett, N. Lo Iudice, A. V. Sushkov, L. Bettermann, N. Braun, D. G. Burke, G. A. Demand, T. Faestermann, P. Finlay, K. L. Green, R. Hertenberger, K. G. Leach, R. Krücken, M. A. Schumaker, C. E. Svensson, H.-F. Wirth, and J. Wong, Phys. Rev. C **82**, 034321 (2010).
[22] F. Todd Baker, A. Sethi, V. Penumetcha, G. Emery, W. Jones, M. Grimm, and M. Whiten, Nucl. Phys. A **501**, 546 (1989).

[23] D. G. Burke, M. A. M. Shahabuddin, and R. N. Boyd, Phys. Lett. B **78**, 48 (1978).
[24] F. Todd Baker, M. A. Grimm, Jr., A. Scott, R. C. Styles, T. H. Kruse, K. Jones, and R. Suchannek, Nucl. Phys. A **371**, 68 (1981).
[25] J. M. Allmond, R. Zaballa, A. M. Oros-Peusquens, W. D. Kulp, and J. L. Wood, Phys. Rev. C **78**, 014302 (2008).
[26] J. L. Wood, A. M. Oros-Peusquens, R. Zaballa, J. M. Allmond, and W. D. Kulp, Phys. Rev. C **70**, 024308 (2004).
[27] G. Gervais, D. C. Radford, Y. R. Shimizu, M. Cromaz, J. DeGraaf, T. E. Drake, S. Flibotte, A. Galindo-Uribarri, D. S. Haslip, V. P. Janzen, M. Matsuzaki, S. M. Mullins, J. M. Nieminen, C. E. Svensson, J. C. Waddington, D. Ward, and J. N. Wilson, Nucl. Phys. A **624**, 257 (1997).
[28] R. B. Yadav, W. C. Ma, J. C. Marsh, Q. A. Ijaz, R. V. F. Janssens, M. P. Carpenter, C. R. Hoffman, T. Lauritsen, S. Zhu, F. G. Kondev, G. Gurdal, G. B. Hagemann, D. J. Hartley, L. L. Riedinger, and S. Mukhopadhyay, Phys. Rev. C **90**, 054325 (2014).
[29] J. F. Sharpey-Schafer, T. E. Madiba, S. P. Bvumbi, E. A. Lawrie, J. J. Lawrie, A. Minkova, S. M. Mullins, P. Papka, D. G. Roux, and J. Timár, Eur. Phys. J. A **47**, 6 (2011).
[30] M. A. Sithole, J. F. Sharpey-Schafer, E. A. Lawrie, S. N. T. Majola, A. Kardan, T. D. Bucher, J. J. Lawrie, L. Mdletshe, S. S. Ntshangase, A. A. Netshiya, and P. Jones, L. Makhathini, K. L. Malatji, P. L. Masiteng, I. Ragnarsson, B. Maqabuka, J. Ndayishimye, O. Shirinda, B. R. Zikhali, S. Jongile *et al.*, Phys. Rev. C **103**, 024325 (2021).
[31] J. F. Sharpey-Schafer, Nucl. Phys. News Int. **14**, 5 (2004).
[32] B. Harmatz, T. H. Handley, and J. W. Mihelich, Phys. Rev. **128**, 1186 (1962).
[33] W. B. Ewbank, Nucl. Data B **1**, 23 (1966).
[34] K. Ahlgren and P. J. Daly, Nucl. Phys. A **189**, 368 (1972).
[35] P. Morgen, B. S. Nielsen, J. Onsgaard, and C. Søndergaard, Nucl. Phys. A **204**, 81 (1973).
[36] R. Thompson and R. K. Sheline, Phys. Rev. C **7**, 1247 (1973).
[37] H. L. Sharma and N. M. Hintz, Phys. Rev. C **13**, 2288 (1976).
[38] A. M. Bruce, C. Thwaites, W. Gelletly, D. D. Warner, S. Albers, M. Eschenauer, M. Schimmer, and P. von Brentano, Phys. Rev. C **56**, 1438 (1997).
[39] R. Sahu, M. Satpathy, and L. Satpathy, Phys. Rev. C **23**, 1777 (1981).
[40] H. Sodan, W. D. Fromm, L. Funke, K. H. Kaun, P. Kemnitz, E. Will, G. Winter, and J. Berzins, Nucl. Phys. A **237**, 333 (1975).
[41] S. G. Malmskog, V. Berg, B. Fogelberg, and A. Bäcklin, Nucl. Phys. A **166**, 573 (1971).
[42] T. W. Conlon, Nucl. Phys. A **100**, 545 (1967).
[43] T. Shizuma, K. Matsuura, Y. Toh, Y. Hayakawa, M. Oshima, Y. Hatsukawa, M. Matsuda, K. Furuno, Y. Sasaki, T. Komatsubara, and Y. R. Shimizu, Nucl. Phys. A **696**, 337 (2001).
[44] T. Shizuma, S. Mitarai, G. Sletten, R. A. Bark, N. L. Gjørup, H. J. Jensen, M. Piiparinen, J. Wrzesinski, and Y. R. Shimizu, Phys. Rev. C **69**, 024305 (2004).
[45] R. Bengtsson, S. Frauendorf, and F. R. May, At. Data Nucl. Data Tables **35**, 15 (1986).
[46] B. G. Carlsson, I. Ragnarsson, R. Bengtsson, E. O. Lieder, R. M. Lieder, and A. A. Pasternak, Phys. Rev. C **78**, 034316 (2008).
[47] H. L. Ma, B. G. Carlsson, I. Ragnarsson, and H. Ryde, Phys. Rev. C **90**, 014316 (2014).
[48] T. Bengtsson, Nucl. Phys. A **496**, 56 (1989).
[49] T. Bengtsson and I. Ragnarsson, Nucl. Phys. A **436**, 14 (1985).
[50] S. G. Nilsson, C. F. Tsang, A. S. Z. Szymanski, S. Wycech, C. Gustafson, I.-L. Lamm, P. Moller, and B. Nilsson, Nucl. Phys. A **131**, 1 (1969).
[51] E. A. Lawrie, O. Shirinda, and C. M. Petrache, Phys. Rev. C **101**, 034306 (2020).